

# Implementation Of Decoders for LDPC Block Codes and LDPC Convolutional Codes Based on GPUs

Yue Zhao, Francis Lau, *Senior Member, IEEE*

## I. INTRODUCTION

**L**OW-DENSITY parity-check (LDPC) codes were invented by Robert Gallager [1] but had been ignored for years until Mackay rediscovered them [2]. They have attracted much attention recently because they can achieve excellent error performance based on the belief propagation (BP) decoding algorithm.

However, the BP decoding algorithm requires intensive computations. For applications like optical communication [3], [4] which requires BERs down to  $10^{-15}$ , using CPU-based programs to simulate the LDPC decoder is simply impractical. Fortunately, the decoding algorithm possesses a high data-parallelism feature, i.e., the data used in the decoding process are manipulated in a very similar manner and can be processed separately from one another. Thus, practical decoders with low-latency and high-throughput can be implemented with dedicated hardware such as field programmable gate arrays (FPGAs) or application specific integrated circuits (ASICs) [5], [6], [7]. However, high performance FPGAs and ASICs are very expensive and are non-affordable by most researchers. Such hardware solutions also cost a long time to develop. In addition, the hardware control and interconnection frame are always associated with a specific LDPC code. If one parameter of an LDPC code/decoder changes, the corresponding hardware design has to be changed accordingly, rendering the hardware-based solutions non-flexible and non-scalable.

Recently, graphics processing units (GPUs) used to process graphics only have been applied to support general purpose computations [8]. In fact, GPUs are highly parallel structures with many processing units. They support floating point arithmetics and can hence conduct computations with the same precision as CPUs. GPUs are particularly efficient in carrying out the same operations to a large amount of (different) data. Compared with modern CPUs, GPUs can also provide much higher data-parallelism and bandwidth.

Yue Zhao and Francis Lau are with the Department of Electronic and Information Engineering, The Hong Kong Polytechnic University.

Consequently, GPUs can provide a cheap, flexible and efficient solution of simulating a LDPC decoder. Potentially, the simulation time can be reduced from several days to a few hours when GPUs, instead of CPUs, are used. In addition, the GPU programming codes can be re-used without much modification should more advanced GPUs are produced by manufacturers.

In [9], [10], a compressed parity-check matrix has been proposed to store the indices of the passing messages in a cyclic or quasi-cyclic LDPC code. Further, the matrix is stored in the constant cache memory on the GPU for fast access. The messages are stored in a compressed manner such that the global memory can be accessed in a coalesced way frequently. However, the coalesced memory access occurs only during the data-read process and is not always guaranteed due to a lack of data alignment. In [11], [8], the sum-product LDPC decoder and the min-sum decoder have been implemented with GPUs. Moreover, by combining sixteen fixed-point 8-bit data to form one 128-bit data, the LDPC decoder in [8] decodes sixteen codewords simultaneously and achieves a high throughput. Although the method in [8] allows coalesced memory access in *either* the read *or* write process, coalesced memory access in *both* the read *and* write processes is yet to be achieved.

Furthermore, the LDPC convolutional codes (LDPCCCs), first proposed in [12], have been shown to achieve a better error performance than the LDPC block code counterpart of similar decoding complexity. There are many features of LDPCCC that make it suitable for real applications. First, the LDPCCC inherits the structure of the convolutional code, which allows continuous encoding and decoding of variable-length codes. Thus the transmission of codewords with varying code length is possible. Second, the LDPCCC adopts a pipelined decoding architecture — in the iterative decoding procedure, each iteration is processed by a separate processor and the procedure can be performed in parallel. So a high-throughput decoder architecture is possible. In [13], [14], the concepts and realization of highly parallelized decoder architectures have been presented and discussed. To the author's best knowledge, there is not any GPU-based implementation of the LDPCCC decoder yet. The reason may lie in the complexity structure of the LDPCCC compared to the LDPC block code, particularly the random time-varying LDPCCC.

As will be discussed in this paper, a LDPCCC derived from a well designed QC-LDPC code possesses not only the good BER performance, but also the regular structure that results in many advantages in practical implementations. Due to the structure inherited from the QC-LDPC code, the LDPCCC decoder enables an efficient and compact memory storage of the messages with a simple address controller.

In this paper, we develop flexible and highly parallel GPU-based decoders for the LDPC codes. The decoder is divided into two sub-types — one using the standard BP algorithm (called Type-A decoder) and another using layered decoding algorithm (called Type-B decoder). We improve the efficiency by making (i) the threads of a warp follow the same execution path and (ii) the memory accessed by a warp

be of a certain size and be aligned. The results show that the decoders based on the GPUs achieve the same BER performance as the CPU-based ones but the speed-up is remarkable: the Type-A decoder is more than 100 times faster than the CPU one while the Type-B decoder is even faster.

We also develop a GPU-based decoder for the LDPC convolutional codes. We propose a decoder architecture for LDPCCC derived from QC-LDPC block-code. By taking advantage of the homogeneous operations of the pipeline processors, we compress the index information of different processors into one lookup table. Combined with an efficient thread layout, the decoder is optimized in terms of thread execution and memory access. The GPU simulation results show that the LDPCCCs have better bit error performance than their block-code counterpart. Moreover, compared to the CPU-based decoder, the GPU-based one can achieve as many as 200 times speed-up.

The rest of the paper is organized as follows. Section II reviews the structure and decoding algorithm of the LDPC code. The same section also reviews the construction of LDPCCC based on QC-LDPC code as well as the decoding process for the LDPCCC. In Section III, the architecture of CUDA GPU and the CUDA programming model is introduced. Section IV describes the implementation of the LDPC decoder and LDPCCC decoder based on GPUs. Section V presents the simulation results of the LDPC decoder and LDPCCC decoder. Both the BER performance and decoding time performance are compared with the CPU ones. Finally, Section VI concludes the paper.

## II. REVIEW OF LDPC CODES AND LDPC CONVOLUTIONAL CODES

### A. Structure of LDPC Codes and QC-LDPC Codes

A binary  $(N, K)$  LDPC code is a linear block code specified by a sparse  $M \times N$  parity-check matrix  $\mathbf{H}$ , where  $M = N - K$ . The code rate of such an LDPC code is  $R \geq K/N = 1 - M/N$ . The equality holds when  $\mathbf{H}$  is full rank.

The  $\mathbf{H}$  matrix contains mostly 0's and relatively a small number of 1's. Such a sparsity structure is the key characteristic that guarantees good performance of LDPC codes. A *regular* LDPC code is a linear block code with  $\mathbf{H}$  containing a constant number  $w_c$  of 1's in each column and a constant number  $w_r$  of 1's in each row. Moreover,  $w_r$  and  $w_c$  satisfy the equation  $w_r = w_c \times \frac{N}{M}$ . Otherwise the code is defined as an *irregular* LDPC code.

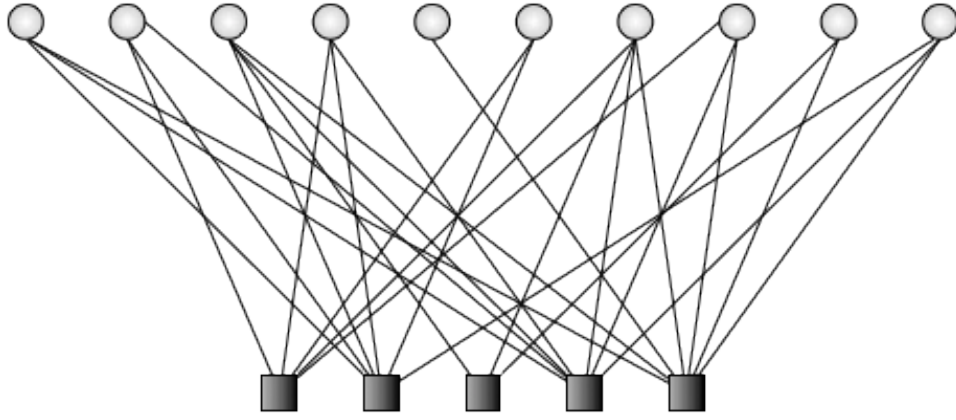


Fig. 1: Tanner Graph representation of the LDPC code defined by (1)

**Example 1.** The parity-check matrix  $\mathbf{H}$  in (1) shows an example of an irregular LDPC code.

$$\mathbf{H} = \begin{bmatrix} 1 & 1 & 1 & 1 & 0 & 1 & 0 & 1 & 0 & 1 \\ 1 & 0 & 1 & 1 & 0 & 0 & 1 & 1 & 1 & 1 \\ 0 & 1 & 0 & 1 & 0 & 0 & 0 & 1 & 0 & 0 \\ 1 & 0 & 0 & 0 & 1 & 0 & 1 & 1 & 1 & 1 \\ 0 & 0 & 1 & 1 & 1 & 0 & 1 & 0 & 1 & 0 \end{bmatrix} \quad (1)$$

A bipartite graph called Tanner graph [15] can be used to represent the codes and to visualize the message-passing algorithm. Fig. 1 is the underlying Tanner graph of the  $\mathbf{H}$  in (1). The  $N$  nodes on the left are called the message nodes or the variable nodes and the  $M$  nodes on the right are called the check nodes. An edge in the Tanner graph represents the adjacency of the variable node  $i$  and the check node  $j$ . It corresponds to a nonzero  $(i, j)$ -th entry in the  $\mathbf{H}$  matrix.

QC-LDPC codes form a subclass of LDPC codes with the parity-check matrix consisting of circulant permutation matrices [16], [17]. The parity-check matrix of a regular  $(J, L)$  QC-LDPC code is represented by

$$\mathbf{H} = \begin{bmatrix} \mathbf{P}^{a_{1,1}} & \mathbf{P}^{a_{1,2}} & \dots & \mathbf{P}^{a_{1,L}} \\ \mathbf{P}^{a_{2,1}} & \mathbf{P}^{a_{2,2}} & \dots & \mathbf{P}^{a_{2,L}} \\ \vdots & \dots & \dots & \vdots \\ \mathbf{P}^{a_{J,1}} & \mathbf{P}^{a_{J,2}} & \dots & \mathbf{P}^{a_{J,L}} \end{bmatrix}, \quad (2)$$

where  $J$  denotes the number of block rows,  $L$  is the number of block columns,  $\mathbf{P}$  is the identity matrix of size  $p \times p$ , and  $\mathbf{P}^{a_{j,l}}$  ( $1 \leq j \leq J$ ;  $1 \leq l \leq L$ ) is a circulant matrix formed by shifting the columns of  $\mathbf{P}$  cyclically to the right  $a_{j,l}$  times with  $a_{j,l}$ 's being non-negative integers less than  $p$ . The code rate  $R$  of  $\mathbf{H}$  is lower bounded by  $R \geq 1 - J/L$ . If one or more of the sub-matrix(matrixes) is/are substituted by the zero matrix rendering non-uniform distributions of the check-node degrees or variable-node degrees, the QC-LDPC code becomes an irregular code.

## B. Decoding Algorithm for LPDC Codes

1) *The standard Belief Propagation Algorithm:* LDPC codes are most commonly decoded using the belief propagation (BP) algorithm [18], [19]. Referring to the Tanner graph shown in Fig. 1, the variable nodes and the check nodes exchange soft messages iteratively based on the connections and according to a two-phase schedule.

Given a binary  $(N, K)$  LDPC code with a parity-check matrix  $\mathbf{H}$ , we define  $\mathcal{C}$  as the set of binary codewords  $\mathbf{c}$  that satisfy the equation  $\mathbf{c}\mathbf{H}^T = \mathbf{0}$ . At the transmitter side, a binary codeword  $\mathbf{c} = (c_0, c_1, \dots, c_{N-1})$  is mapped into the sequence  $\mathbf{x} = (x_0, x_1, \dots, x_{N-1})$  according to  $x_n = 1 - 2c_n$ . We assume that  $\mathbf{x}$  is then transmitted over an additive white Gaussian noise (AWGN) channel and the received signal vector is then given by  $\mathbf{y} = (y_0, y_1, \dots, y_{N-1}) = \mathbf{x} + \mathbf{g}$ , where  $\mathbf{g} = (g_0, g_1, \dots, g_{N-1})$  consists of independent Gaussian random variables with zero mean and variance  $\sigma^2 = N_0/2$ .

Let  $\mu_n$  be the initial log-likelihood ratio (LLR) that the variable node  $n$  is a “0” to that it is a “1”, i.e.,

$$\mu_n = \ln \left( \frac{\Pr(c_n = 0|y_n)}{\Pr(c_n = 1|y_n)} \right) \quad (3)$$

Initially,  $\mu_n$  is calculated by  $\mu_n = (4/N_0) \cdot y_n = \frac{2y_n}{\sigma^2}$  [20]. Define  $\mathcal{N}(m)$  as the set of variable nodes that participate in check node  $m$  and  $\mathcal{M}(n)$  as the set of check nodes connected to variable node  $n$ . At iteration  $i$ , let  $\beta_{mn}^{(i)}$  be the LLR messages passed from variable node  $n$  to check node  $m$ ;  $\alpha_{mn}^{(i)}$  be the LLR messages passed from check node  $m$  to variable node  $n$ ; and  $\beta_n^{(i)}$  be the *a posteriori* LLR of variable node  $n$ . Then the standard BP algorithm can be described as follows [2], [21].

- 1) Initialization:  $\beta_{mn}^{(0)} = \mu_n$  for  $0 \leq n \leq N - 1$  and  $m \in \mathcal{M}(n)$ . We set the iteration number  $i = 1$  and the maximum number of iterations to  $I_{max}$ .
- 2) Iteration: First, the variable-node messages  $\beta_{mn}^{(i-1)}$ 's are passed to check nodes. Then the check nodes use these incoming messages  $\beta_{mn}^{(i-1)}$ 's to update the outgoing messages  $\alpha_{mn}^{(i)}$ 's. Second,  $\alpha_{mn}^{(i)}$ 's are passed to variable nodes from check nodes so as to calculate the  $\beta_{mn}^{(i)}$ 's for the next iteration.

- a) Horizontal Step: For  $0 \leq m \leq M - 1$  and for  $n \in \mathcal{N}(m)$ , the check-to-variable messages are updated by

$$\alpha_{mn}^{(i)} = 2 \tanh^{-1} \left( \prod_{n' \in \mathcal{N}(m) \setminus n} \tanh \left( \frac{\beta_{mn'}^{(i-1)}}{2} \right) \right) \quad (4)$$

where  $\mathcal{N}(m) \setminus n$  denotes the set  $\mathcal{N}(m)$  excluding the variable node  $n$ .

- b) Vertical Step: For  $0 \leq n \leq N - 1$  and  $m \in \mathcal{M}(n)$ , the variable-to-check messages are calculated by

$$\beta_{mn}^{(i)} = \mu_n + \sum_{m' \in \mathcal{M}(n) \setminus m} \alpha_{m'n}^{(i)} \quad (5)$$

and the *a posteriori* LLRs are evaluated using

$$\beta_n^{(i)} = \mu_n + \sum_{m' \in \mathcal{M}(n)} \alpha_{m'n}^{(i)} \quad (6)$$

where  $\mathcal{M}(n) \setminus m$  denotes the set  $\mathcal{M}(n)$  with check node  $m$  excluded.

- 3) Hard decision and stopping condition: At the end of each iteration, the variable nodes will make hard decisions based on the updated *a posteriori* LLRs, i.e.,

$$\hat{c}_n^{(i)} = \begin{cases} 0 & \text{if } \beta_n^{(i)} \geq 0 \\ 1 & \text{if } \beta_n^{(i)} < 0 \end{cases}. \quad (7)$$

If the decoded codeword  $\hat{\mathbf{c}}^{(i)} = (\hat{c}_0^{(i)}, \hat{c}_1^{(i)}, \dots, \hat{c}_{N-1}^{(i)})$  is a valid codeword, i.e.,  $\hat{\mathbf{c}}^{(i)} \mathbf{H}^T = \mathbf{0}$ , or the maximum number of iterations  $I_{max}$  is reached, the decoding operation will stop; otherwise the iteration number  $i$  will be incremented and Steps 2) and 3) will be repeated.

2) *The layered Decoding Algorithm:* In [22], another iterative decoding approach referred to as layered decoding is presented. It is shown to converge about two times faster than the standard BP algorithm [21]. In the layered decoding algorithm, the variable nodes only keep the *a posteriori* LLRs. At each iteration, for each check node  $m$ , the incoming messages along all incident edges from the neighboring variable nodes are computed first. Since the incoming messages should be the extrinsic information, they are obtained by subtracting the previous check-to-variable message along that edge from the *a posteriori* LLR of the associated variable node. Then check node  $m$  can update the outgoing messages along each edge. After this, all neighboring variable nodes of check node  $m$  will update their *a posteriori* LLRs with the newly updated check-to-variable message. The detailed procedure can be formulated by the following steps and equations.

First, the *a posteriori* LLR  $\beta_n^{(0)}$  is initialized as the channel messages. Then the following iteration is repeated for every check node:

$$\beta_{mn}^{(i)} = \beta_n^{(i-1)} - \alpha_{mn}^{(i-1)}, \quad n \in \mathcal{N}(m) \quad (8)$$

$$\alpha_{mn}^{(i)} = 2 \tanh^{-1} \prod_{n' \in \mathcal{N}(m) \setminus n} \tanh\left(\frac{\beta_{mn'}^{(i)}}{2}\right) \quad (9)$$

$$\beta_n^{(i)} = \beta_{mn}^{(i)} + \alpha_{mn}^{(i)}, \quad n \in \mathcal{N}(m) \quad (10)$$

In each iteration, the horizontal step and vertical step will be processed jointly. It is also observed that the check nodes connected to the same variable node must be processed in sequence while in standard BP decoding they can be fully processed in parallel. To exploit the parallelism advantage of the BP algorithm for layered decoding, the rows of the parity-check matrix of an LDPC code are divided into



A code sequence  $\mathbf{v}_{[0,\infty]} = [\mathbf{v}_0, \mathbf{v}_1, \dots, \mathbf{v}_\infty]$  is “valid” if it satisfies the equation

$$\mathbf{v}_{[0,\infty]} \mathbf{H}_{[0,\infty]}^T = \mathbf{0} \quad (11)$$

where  $\mathbf{v}_i = (v_i^{(1)}, v_i^{(2)}, \dots, v_i^{(c)})$  and  $\mathbf{H}_{[0,\infty]}^T$  is the syndrome-former (transposed parity-check) matrix of  $\mathbf{H}_{[0,\infty]}$ .

#### D. Deriving LDPC Convolutional codes from QC-LDPC block codes

There are several methods to construct LDPC convolutional codes from LDPC block codes. One method is to derive time-varying LDPCCC by unwrapping randomly constructed LDPC block codes [12] and another is by unwrapping the QC-LDPC codes [23], [24]. We now consider a construction method by unwrapping a class of QC-LDPC block code.

Suppose we have created a  $(J, L)$  QC-LDPC block code  $\mathbf{H}_{QC}$  with  $J$  block-rows and  $L$  block-columns. The size of its circulant matrices is  $p \times p$ . We can derive the parity-check matrix for a LDPC convolutional code using the following steps.

- 1) Partition the  $pJ \times pL$  parity-check matrix  $\mathbf{H}_{QC}$  to form a  $\Lambda \times \Lambda$  matrix, where  $\Lambda$  is the greatest common divisor of  $J$  and  $L$ , i.e.,

$$\mathbf{H}_{QC} = \begin{bmatrix} \mathbf{H}_{1,1} & \mathbf{H}_{1,2} & \cdots & \mathbf{H}_{1,\Lambda} \\ \mathbf{H}_{2,1} & \mathbf{H}_{2,2} & \cdots & \mathbf{H}_{2,\Lambda} \\ \vdots & \vdots & \cdots & \vdots \\ \mathbf{H}_{\Lambda,1} & \mathbf{H}_{\Lambda,2} & \cdots & \mathbf{H}_{\Lambda,\Lambda} \end{bmatrix}_{\Lambda \times \Lambda},$$

where  $\mathbf{H}_{i,j}$  is a  $(pJ/\Lambda) \times (pL/\Lambda)$  matrix, for  $i, j = 1, 2, \dots, \Lambda$ .

- 2) Divide  $\mathbf{H}_{QC}$  along the diagonal into two portions: the strictly upper-triangular portion  $\mathbf{H}_{QC}^{(U)}$  and the lower-triangular portion  $\mathbf{H}_{QC}^{(L)}$  as follows:

$$\mathbf{H}_{QC}^{(U)} = \begin{bmatrix} \mathbf{0} & \mathbf{H}_{1,2} & \mathbf{H}_{1,3} & \cdots & \mathbf{H}_{1,\Lambda} \\ & \mathbf{0} & \mathbf{H}_{2,3} & \cdots & \mathbf{H}_{2,\Lambda} \\ & & \ddots & \cdots & \vdots \\ & & & \mathbf{0} & \mathbf{H}_{\Lambda-1,\Lambda} \\ & & & & \mathbf{0} \end{bmatrix}_{\Lambda \times \Lambda},$$

and

$$\mathbf{H}_{QC}^{(L)} = \begin{bmatrix} \mathbf{H}_{1,1} & & & & \\ \mathbf{H}_{2,1} & \mathbf{H}_{2,2} & & & \\ \vdots & \vdots & \ddots & & \\ \mathbf{H}_{\Lambda,1} & \mathbf{H}_{\Lambda,2} & \cdots & \mathbf{H}_{\Lambda,\Lambda} & \end{bmatrix}_{\Lambda \times \Lambda}.$$

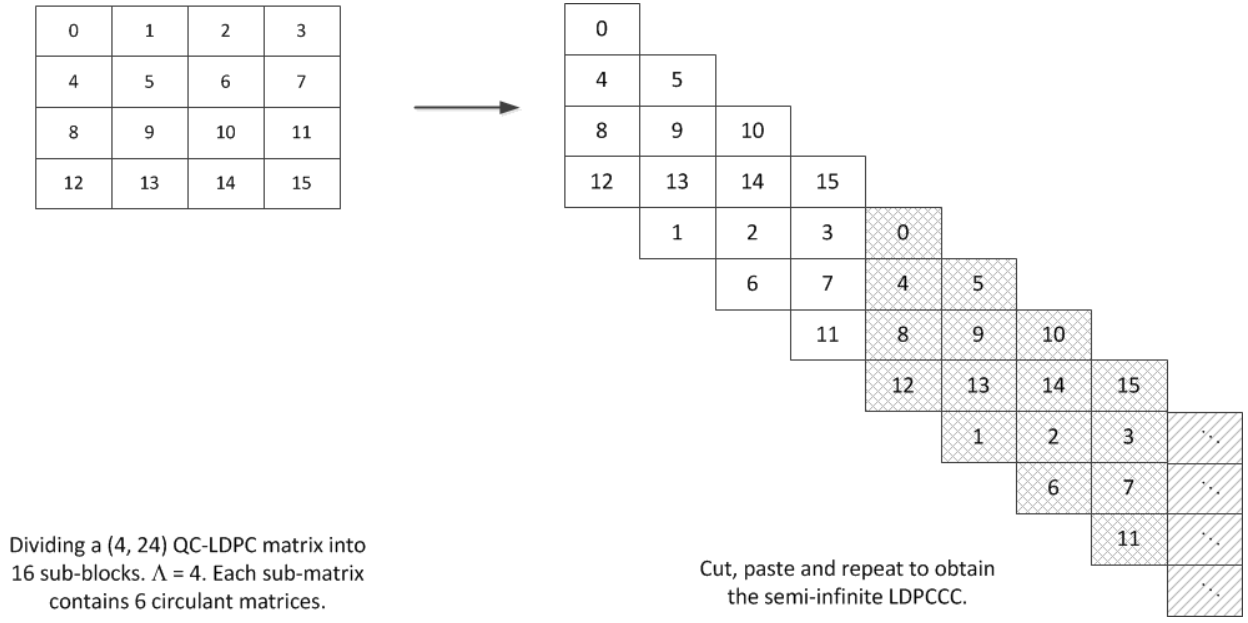


Fig. 2: Illustration of constructing a LPDCCC from a QC-LDPC block code.

- 3) Unwrap the parity-check matrix of the block code to obtain the parity-check matrix of LPDCCC. First paste the strictly upper-triangular portion below the lower-triangular portion. Then repeat the resulting diagonally-shaped matrix infinitely, i.e.,

$$\mathbf{H}_{conv} = \begin{bmatrix} \mathbf{H}_{QC}^L & & & & & \\ \mathbf{H}_{QC}^U & \mathbf{H}_{QC}^L & & & & \\ & \mathbf{H}_{QC}^U & \mathbf{H}_{QC}^L & & & \\ & & \mathbf{H}_{QC}^U & \mathbf{H}_{QC}^L & & \\ & & & \ddots & \ddots & \\ & & & & \ddots & \ddots \end{bmatrix}.$$

The resulting time-varying LPDCCC has a period of  $T = \Lambda$  and the memory  $m_s$  equals  $\Lambda - 1$ . The girth of the derived LPDCCC is at least as large as the girth of the QC-LDPC code [25]. A convenient feature of this time-varying unwrapping is that a family of LDPC convolutional codes can be derived by choosing different circulant size  $p$  of the QC-LDPC block code.

**Example 2.** Consider a (4, 24) QC-LDPC code with the parity-check matrix. It is first divided into  $4 \times 4$  equally sized sub-blocks<sup>1</sup>, i.e.,  $\Lambda = 4$ . Then the parity-check matrix of LPDCCC is derived. The construction process is shown in Fig. 2.

### E. Decoding Algorithm for LPDCCC

In  $\mathbf{H}_{[0,\infty]}$ , two different variable nodes connected to the same check node cannot be distant from each other more than  $m_s$  time units. This allows a decoding window that operates on a fixed number of nodes

<sup>1</sup>Here we use sub-block to denote the  $(pJ/\Lambda) \times (pL/\Lambda)$  matrix as to distinguish it with the sub-matrix within it, i.e., the  $p \times p$  matrix.

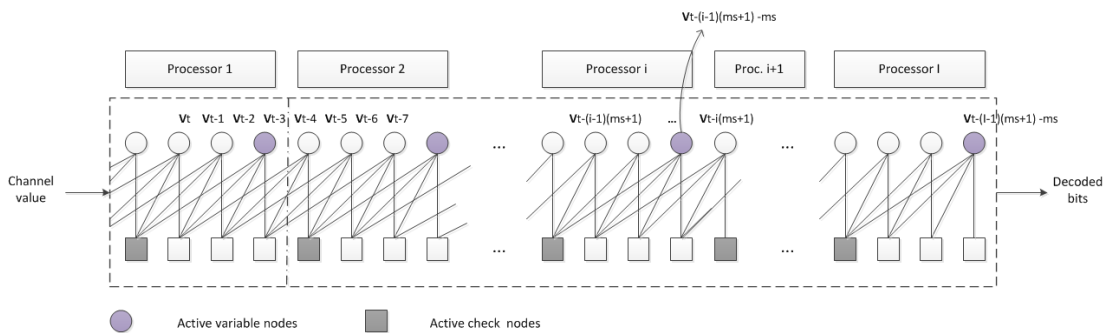


Fig. 3: Continuous decoding of LDPC convolutional code with  $I$  processors. Each circle denotes a group of  $c$  variable nodes and each square denotes a group of  $(c - b)$  check nodes. Each edge represents the connection between the  $c$  variable node and the  $(c - b)$  check nodes.

at one time. Since any two variable nodes that are at least  $m_s + 1$  units apart can be decoded independently, parallel implementation is feasible. The LDPCCC can therefore be decoded with pipelined belief propagation decoding algorithm [12]. Specifically, for a maximum iteration number of  $I$ ,  $I$  independent processors will be employed working on different variable nodes corresponding to different time.

Fig. 3 shows a decoder on the Tanner graph based on the LDPCCC structure in Example 2 with rate  $R = 5/6$  and syndrome former memory  $m_s = 3$ . We refer the  $c$  incoming variable nodes (bits) as a frame. Note that every  $c$  bits form a frame and every  $m_s + 1$  frames are involved in the same constraints. The  $I$  processors can operate concurrently. At every iteration, every processor first updates the  $(c - b)$  neighboring check nodes of the  $c$  variable nodes that just come into this processor. Then every processor will update the  $c$  variables which are leaving this processor.

The computations of the check-node updating and variable-node updating are based on the standard belief propagation algorithm. Suppose  $\mathbf{v}_{[0,\infty]} = [\mathbf{v}_0, \mathbf{v}_1, \dots, \mathbf{v}_\infty]$ , where  $\mathbf{v}_i = (v_i^{(1)}, v_i^{(2)}, \dots, v_i^{(c)})$  is the transmitted codeword.

At time  $t$ , when a decoding iteration begins,  $c$  variable nodes denoted by  $\mathbf{v}_t$  along with their channel messages  $\mu_n$  enter the first processor. Meanwhile, the variables  $\mathbf{v}_{t-i(m_s+1)}$  along with the associated variable-to-check messages are shifted from the  $i$ -th processor to the  $(i + 1)$ -th processor if  $t \geq i(m_s + 1)$ , where  $i = 1, 2, \dots, I - 1$ . Then every processor  $i$  ( $i = 1, 2, \dots, I$ ) updates the  $(c - b)$  check nodes corresponding to the  $t - (i - 1)(m_s + 1)$ -th block row of  $\mathbf{H}_{[0,\infty]}$  (as in (12)) using

$$\alpha_{mn} = 2 \tanh^{-1} \left( \prod_{n' \in \mathcal{N}(m) \setminus n} \tanh \left( \frac{\beta_{mn'}}{2} \right) \right) \quad (12)$$

Next, each processor will update the corresponding variable nodes  $\mathbf{v}_{t-(i-1)(m_s+1)-m_s}$  where  $i = 1, 2, \dots, I$

as follows,

$$\beta_{mn} = \mu_n + \sum_{m' \in \mathcal{M}(n) \setminus m} \alpha_{m'n} \quad (13)$$

Finally, hard decision will be made on the frame of  $c$  variable-nodes leaving the last processor, i.e.,  $\mathbf{v}_{t-(I-1)(m_s+1)-m_s}$ . The decision results are the outputs of the LDPC decoder.

### III. GRAPHICS PROCESSING UNIT AND CUDA PROGRAMMING

In this section, we introduce Nvidia's GPU architecture and its features for effective parallel computing. A graphics processing unit (GPU) consists of multi-threaded, multi-core processors. GPUs follow the single-instruction multiple-data (SIMD) paradigm. That is to say, given a set of data (regarded as a stream), the same operation or function is applied to each element in the stream by different processing units in the GPUs simultaneously. Figure 4 shows a simplified architecture of the latest GPU device. It contains a number of multiprocessors called streaming multiprocessors (or SMs). Each SM contains a group of stream processors or cores and several types of memory including registers, on-chip memory, L2 cache and the most plentiful dynamic random-access memory (DRAM). The L1 cache is dedicated to each multiprocessor and the L2 cache is shared by all multiprocessors. Both caches are used to cache accesses to local or global memory. The on-chip memory has a small capacity (tens of KB) but it has a low latency [26].

In our work, the GPU used is GTX460, which has 7 SMs and 768 MB global memory. Each SM contains 48 cores [27]. Moreover, the 64 KB on-chip memory is configured as 48 KB shared memory and 16 KB L1 cache for each SM because the more shared memory is utilized, the better.

CUDA (Compute Unified Device Architecture) is a parallel computing architecture developed by Nvidia. In a CUDA program, computations are performed as a sequence of functions called parallel kernels. Each kernel is typically invoked on a massive number of threads. Threads are first grouped into thread blocks and blocks are further grouped into a grid. A thread block contains a set of concurrently executing threads, and the size of all blocks are the same with an upper limit  $\Omega_{\max}$ . In the current GPUs,  $\Omega_{\max} = 1024$ .

In an abstract level, the CUDA devices use different memory spaces, which have different characteristics. These memory spaces includes global memory, local memory, shared memory, constant memory, texture memory, and registers. The global memory and texture memory are the most plentiful but have the largest access latency followed by constant memory, registers, and shared memory.

CUDA's hierarchy of threads map to a hierarchy of processors on the GPU. A GPU executes one or more kernel grids and a SM executes one or more thread blocks. The SM creates, manages, schedules, and executes threads in groups of 32 parallel threads called *warps*. A warp is the execution unit and

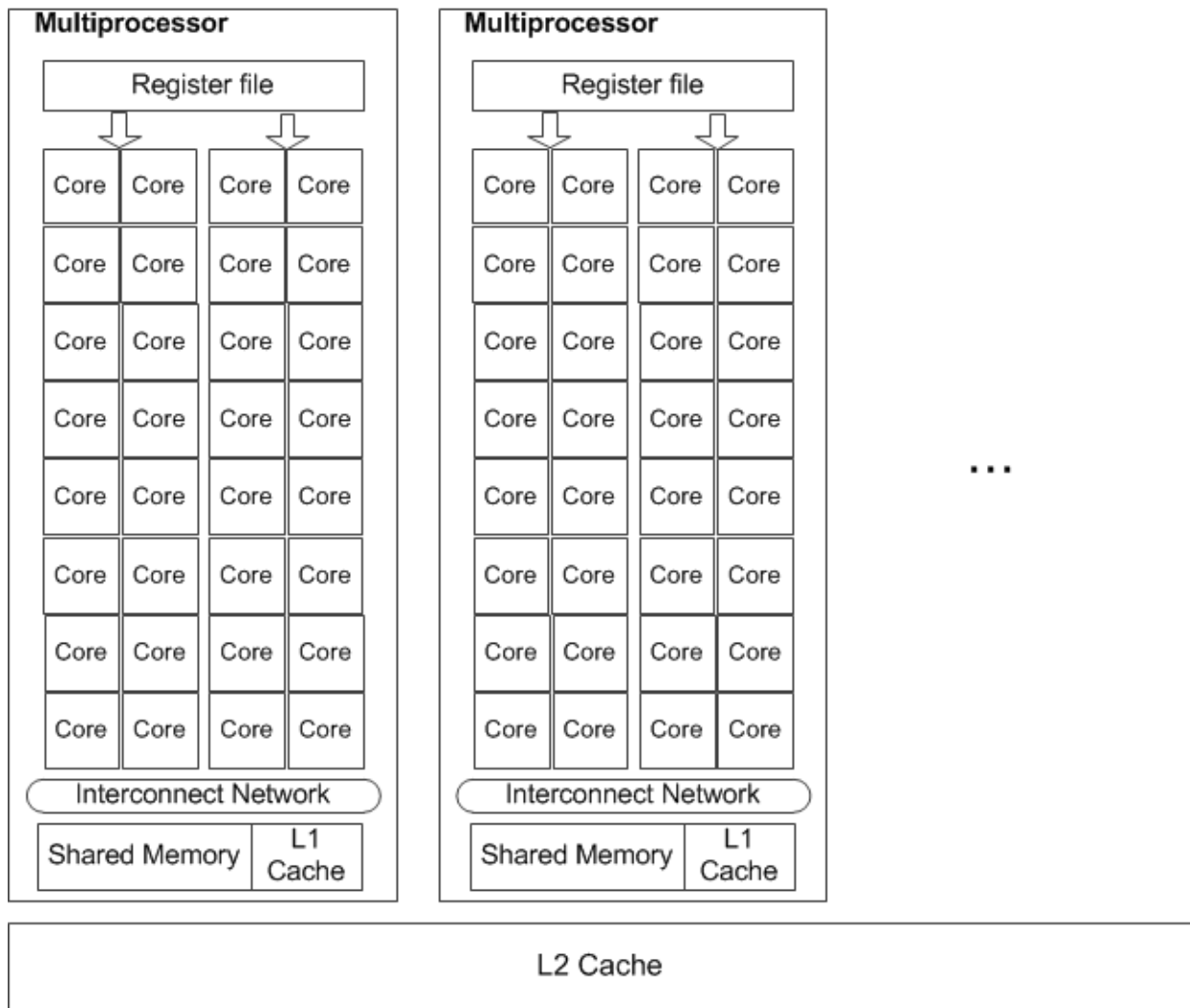


Fig. 4: Hardware architecture of a typical GPU. Each large rectangle denotes a streaming multiprocessor (SM) and each small square in a SM represents a stream processor or core.

executes one common instruction at a time. So full efficiency is realized when threads of a warp take the same execution path.

In CUDA programming, the data throughput has a great impact on the performance. The first important consideration is hence the coalescing global memory accesses. Global memory resides in the device memory and is accessed via 32-, 64-, or 128-byte memory transactions. These memory transactions must be naturally aligned (i.e. the first address is a multiple of their size).

When a warp executes an instruction that accesses the global memory, it coalesces the memory accesses of the threads within the warp into one or more of these memory transactions depending on the size of the word accessed by each thread and the distribution of the memory addresses across the threads.

## IV. IMPLEMENTATION OF DECODERS FOR LDPC CODES AND LDPCCCS

### A. The GPU-based LDPC Decoders

According to the CUDA programming model, the granularity of a thread execution and a coalesced memory access is a warp. Full efficiency is realized when all threads in a warp take the same execution path and the coalesced memory access requirement is satisfied. Thus, we propose to decode  $\Gamma$  codewords simultaneously, where  $\Gamma$  is an integer multiple of a warp (i.e., multiple of 32). For each decoding cycle,  $\Gamma$  codewords will be input, decoded, and output together and in parallel.

1) *Decoder Using Standard BP Algorithm:* We first implement our decoder using the standard BP decoding algorithm. We denote this decoder as Type-A LDPC decoder.

#### *Data Structure*

Recall that an LDPC code can be represented by its parity-check matrix or a Tanner graph. A non-zero element in the parity-check matrix corresponds to an edge in the Tanner graph.

In the LDPC decoder, messages are bound to the edges in the Tanner graph (or the 1's in the parity-check matrix  $\mathbf{H}$ ). So we store the messages according to the positions of 1's. Besides, the channel messages corresponding to the variable nodes are required. To reuse the notation, we denote the data structure storing the messages between the variable nodes and the check nodes as  $\mathbf{H}$  while the data structure storing the channel messages as  $\mathbf{V}$ . The difficulty of the CUDA memory arrangement lies on the fact that for practical LDPC codes with good performance, the positions of the 1's are scattered in the parity-check matrix.

First, in the BP decoding procedure, although there are two kinds of messages, namely, the variable-to-check messages and the check-to-variable messages, at every step of the iteration, only one kind of message is needed to be stored, i.e., after the check-node updating step, only the check-to-variable messages  $\alpha$ 's are stored in the  $\mathbf{H}$  and after the variable-node updating step, only the variable-to-check messages  $\beta$ 's are stored in the  $\mathbf{H}$ . Second, in our new decoder architecture,  $\Gamma$  ( $\Gamma$  is a multiple of a warp) codewords are decoded together and hence the messages of  $\Gamma$  codewords are also processed together. We number the distinct codewords as  $0, 1, \dots, \Gamma - 1$  and we use the same notations for the messages as before, i.e.,  $\beta_{mn}(\gamma)$  is the message from variable node  $n$  to check node  $m$  corresponding to the  $\gamma$ -th codeword and  $\alpha_{mn}(\gamma)$  is the message from check node  $m$  to variable node  $n$  corresponding to the  $\gamma$ -th codeword. Since all the  $\Gamma$  codewords messages share the same Tanner graph, messages of the  $\Gamma$  distinct codewords corresponding to the same edge can be grouped into one package and stored linearly. Let  $\mathbf{p}_{mn}$  denote the package corresponding to the edge connecting variable node  $n$  and check node  $m$ . Then in package  $\mathbf{p}_{mn}$ ,  $\beta_{mn}(0), \beta_{mn}(1), \dots, \beta_{mn}(\Gamma - 1)$  or  $\alpha_{mn}(0), \alpha_{mn}(1), \dots, \alpha_{mn}(\Gamma - 1)$  are stored contiguously. This is shown in Figure 5. Different packages  $\mathbf{p}_{mn}$ 's are aligned linearly according to their corresponding positions in the

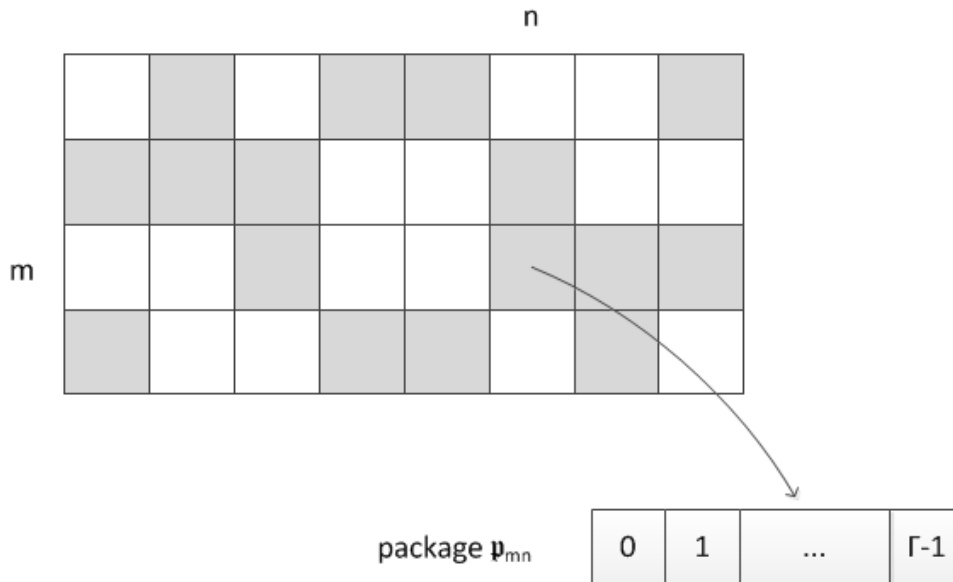


Fig. 5: Data Structure for an LDPC code. The gray square denote the nonzero entry of the parity-check matrix.  $\Gamma$  is a multiple of a warp (i.e., multiple of 32).

parity-check matrix — row-by-row, and left to right for each row. That implies the messages associated to one check node are stored contiguously.

**Remark.** *To be consistent with the use of memory locations in computer programming, all the index of the data structures in the thesis starts from 0.*

The advantage of this arrangement is obvious. Since  $\Gamma$  is a multiple of 32, the memory segment for every package is naturally aligned when the data type belongs to one of the required data types (i.e., with word size of 1-, 2-, 4-, or 8-byte). In addition, the structure of the parity-check matrix  $\mathbf{H}$  is shared by the  $\Gamma$  codewords. As these  $\Gamma$  data elements are processed together, they can be accessed by  $\Gamma$  contiguous threads and hence the global memory is always accessed in a coalesced way. Since  $\Gamma$  is a multiple of a warp and threads within a warp can always follow the same execution path with no divergence occurring. Both the memory access and the thread execution are optimal and efficient.

We also need to store the details of the parity-check matrix. Two lookup tables denoted by  $LUT_c$  and  $LUT_v$  will be kept.  $LUT_c$  is used in the check-node updating process and  $LUT_v$  is used in the variable-node updating process. The two tables store the indices of the data accessed in the two updating processes and both are two-dimensional. The first dimension is to distinguish different check nodes, i.e.,  $LUT_c[m]$  is associated with the  $m$ -th check node or the  $m$ -th row. Each  $LUT_c[m]$  records the indices of the messages related to the  $m$ -th check node. The two lookup tables are shared by all  $\Gamma$  codewords.

**Example 3.** *Consider the parity-check matrix in (14). The corresponding data structure begins with the*

package  $\mathbf{p}_{01}$ , which is followed by  $\mathbf{p}_{03}$ ,  $\mathbf{p}_{04}$ ,  $\mathbf{p}_{07}$ ,  $\mathbf{p}_{10}$ ,  $\mathbf{p}_{11}$ , ...,  $\mathbf{p}_{30}$ , ...,  $\mathbf{p}_{36}$ . The subscripts of the nonzero entries indicate the sequences (or positions) of the associated data in the entire data structure, starting from 0. The  $LUT_c$  and  $LUT_v$  are shown in (15) and (16).

It is seen that the size of  $LUT_c$  can be reduced by only storing the first address of the data in each row, namely,  $LUT_c[0]$  only store 0,  $LUT_c[1]$  only store 4 and so on for all  $m = 0, 1, \dots, M - 1$ . Particularly, for regular LDPC codes with a unique row weight  $d_c$ , the indices in  $LUT_c[m]$  for the  $m$ -th check node are from  $m \cdot d_c$  to  $m \cdot d_c + d_c - 1$ . As for the  $LUT_v$ , the indices are normally irregular and random. Hence a full-indexed lookup table is required for  $LUT_v$ .

The  $LUT_c$  and  $LUT_v$  lookup tables are stored in the constant or texture memory in the CUDA device so as to be cached to reduce the access time.

$$\mathbf{H} = \begin{array}{cccccccc} & \text{variable node } n & & & & & & & \\ & 0 & 1 & 2 & 3 & 4 & 5 & 6 & 7 & \\ \left[ \begin{array}{cccccccc} 0 & 1_{(0)} & 0 & 1_{(1)} & 1_{(2)} & 0 & 0 & 1_{(3)} \\ 1_{(4)} & 1_{(5)} & 1_{(6)} & 0 & 0 & 1_{(7)} & 0 & 0 \\ 0 & 0 & 1_{(8)} & 0 & 0 & 1_{(9)} & 1_{(10)} & 1_{(11)} \\ 1_{(12)} & 0 & 0 & 1_{(13)} & 1_{(14)} & 0 & 1_{(15)} & 0 \end{array} \right] & \begin{array}{l} 0 \\ 1 \\ 2 \\ 3 \end{array} & \text{check node } m \end{array} \quad (14)$$

$$LUT_c = \begin{array}{cccc} \left[ \begin{array}{cccc} 0 & 1 & 2 & 3 \\ 4 & 5 & 6 & 7 \\ 8 & 9 & 10 & 11 \\ 12 & 13 & 14 & 15 \end{array} \right] & \begin{array}{l} 0 \\ 1 \\ 2 \\ 3 \end{array} & \text{check node } m \end{array} \quad (15)$$

$$LUT_v = \begin{array}{ccc} \left[ \begin{array}{cc} 4 & 12 \\ 0 & 5 \\ 6 & 8 \\ 1 & 13 \\ 2 & 14 \\ 7 & 9 \\ 10 & 15 \\ 3 & 11 \end{array} \right] & \begin{array}{l} 0 \\ 1 \\ 2 \\ 3 \\ 4 \\ 5 \\ 6 \\ 7 \end{array} & \text{variable node } n \end{array} \quad (16)$$

A separate thread is assigned to process each check node or each variable node in the updating kernel. Recall that  $\Gamma$  codewords are decoded in parallel and data for the  $\Gamma$  codewords corresponding to the

same edge are grouped into a package. Hence,  $\Gamma$  threads can be assigned to process the data of  $\Gamma$  codewords simultaneously. So, a two dimensional thread hierarchy is launched. The first dimension is for identifying the different codewords while the second dimension is for processing different check nodes or variable nodes. The thread layout is illustrated in Fig. 6. For each thread block, we allocate  $\Gamma$  threads in the  $\text{threadIdx.x}$  dimension<sup>2</sup>, and  $BL_y$  threads in the  $\text{threadIdx.y}$  dimension. Each thread-block contains  $BL_y \times \Gamma$  threads, which should be within the thread-block size limit (1024 for the current device). The total number of thread-blocks is determined by the number of check nodes  $M$  or the number of variable nodes  $N$ . We denote  $BL_y$  in the check-node updating kernel as  $BL_{y,cnu}$  and the one in the variable-node updating kernel as  $BL_{y,vnu}$ . Then the numbers of thread blocks are given by  $\lceil M/BL_{y,cnu} \rceil$  and  $\lceil N/BL_{y,vnu} \rceil$ , respectively. In Fig. 6, the threads marked by the vertical rectangular are processing the same codeword.

In the check-node updating kernel and the variable-node updating kernel, the forward-and-backward calculation is adopted as in [28]. The shared memory is used to cache the involved data as to avoid re-accessing the global memory. Due to the limited size of the shared memory, the size of the thread-block should not be too large. Consider a  $(J, L)$  QC-LDPC code. For each check node, there are  $2L$  data elements to be stored. Denote the shared memory size by  $Z_{\text{shared}}$  and the size of each data by  $Z_{\text{data}}$ . Consequently in the check-node updating kernel, the thread-block size, denoted by  $\Omega_{\text{cnu}}$ , is limited by

$$\Omega_{\text{cnu}} \leq \frac{Z_{\text{shared}}}{2LZ_{\text{data}}}. \quad (17)$$

In addition,  $\Omega_{\text{cnu}} = BL_{y,cnu} \times \Gamma$  and  $\Omega_{\text{vnu}} = BL_{y,vnu} \times \Gamma$ .

With such a thread layout, the threads access the memory in a straightforward pattern. For example, for the check-node updating kernel, a two-dimensional thread hierarchy with a total size of  $\lceil \frac{M}{BL_{y,cnu}} \rceil \times BL_{y,cnu} \times \Gamma$  is launched. During the memory access, every  $\Gamma$  threads are one-to-one mapped to  $\Gamma$  data in a message package. Hence, coalesced memory access is guaranteed.

2) *Decoder Using Layered Decoding Algorithm:* We also implement layered decoding algorithm to reduce the iteration time while obtaining the same BER results. We call this decoder as Type-B decoder. The layered decoding procedure has been introduced in Section II-B2. The parallelism is deployed in each layer.

The data structure for the layered decoder is similar to the one for the Type-A decoder.  $\Gamma$  codewords are decoded together. Data across the  $\Gamma$  codewords are grouped into one package. We denote the data structure of the edge messages as  $\mathbf{H}_{\text{layer}}$  and the data structure of the *a posteriori* LLR messages as  $\mathbf{V}_{\text{layer}}$ . Due to the characteristic of the layered decoding algorithm, only the check-node updating kernel

<sup>2</sup>In CUDA, threads are linear in the  $\text{threadIdx.x}$  dimension.

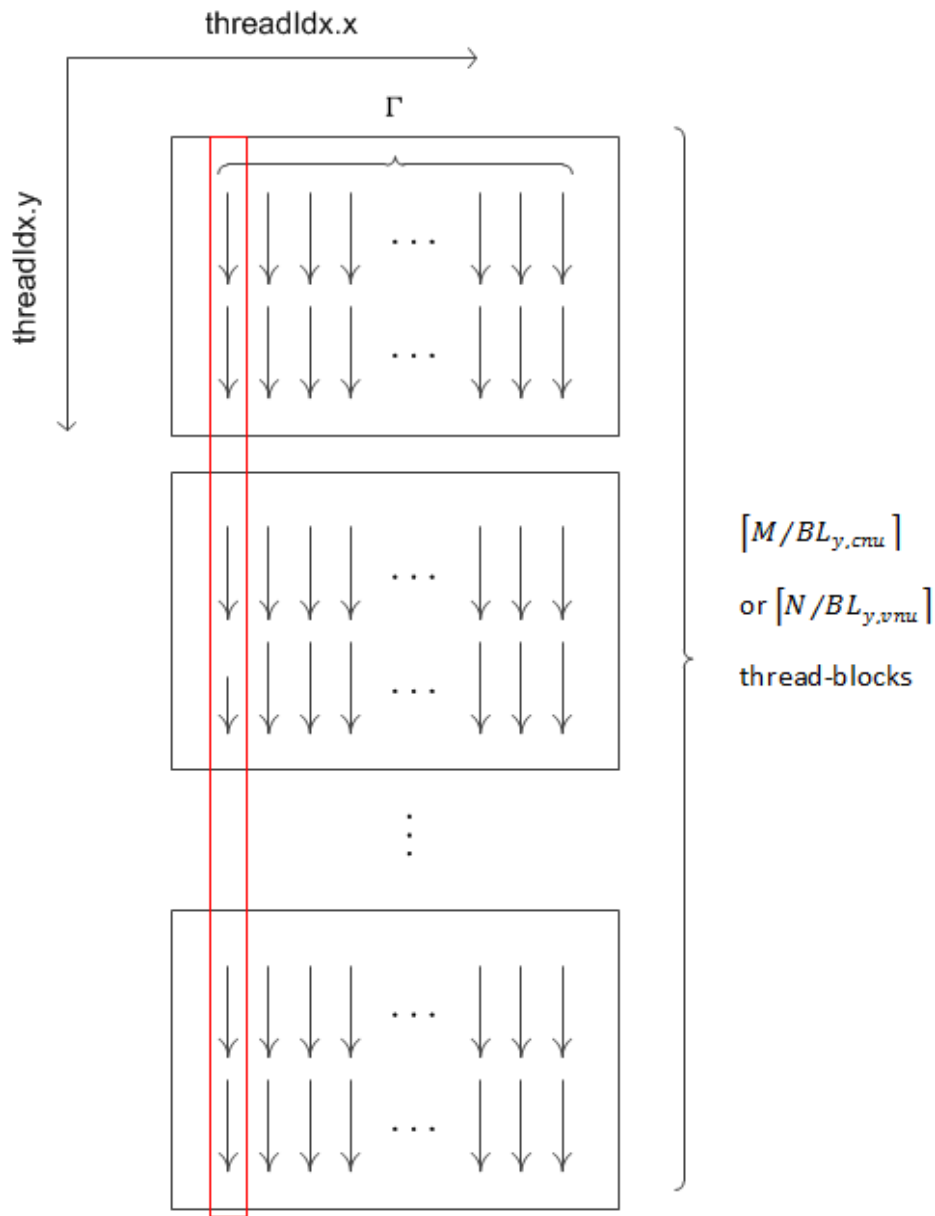


Fig. 6: Two dimensional thread layout of the check-node/variable-node updating kernel.

is needed. So  $\mathbf{H}_{layer}$  only stores the check-to-variable messages while  $\mathbf{V}_{layer}$  always keeps the latest *a posteriori* LLR messages.

The QC-LDPC codes are naturally suitable for the implementation of the layered decoding. For the  $(J, L)$  QC-LDPC code shown in (2), the  $L$  circulant sub-matrices in the same row can be regarded as one layer. The column weight in each layer is at most 1 and a single iteration is performed in each layer. In such a case, each layer contains  $p$  check nodes and the  $p$  check nodes will be processed in parallel. Threads for processing check nodes in one layer, i.e., a total number of  $p \times \Gamma$  threads, are issued. The size of a thread block is  $BL_{y,cnu}^{layered} \times \Gamma$ .

The layered decoding procedures have to be repeated for all the  $J$  layers before one iteration is

completed. A hard decision can be made to check if the estimated codeword satisfies the parity-check equation.

The calculation in (9) adopts the forward-and-backward algorithm as in the BP decoding to exclude the intrinsic information. Thus  $\alpha_{mn}^{(l)}$ 's and  $\beta_{mn}^{(l)}$ 's will be accessed twice. So they will be pre-loaded into the shared memory for reuse. Consequently, for a QC-LDPC code with a row weight of  $L$ ,  $2L$  messages are stored in the shared memory. Then the thread-block size  $\Omega_{\text{cnu}}^{\text{layer}}$  is also limited by

$$\Omega_{\text{cnu}} \leq \frac{Z_{\text{shared}}}{2LZ_{\text{data}}}. \quad (18)$$

Moreover,  $\Omega_{\text{cnu}} = BL_{y,\text{cnu}}^{\text{layer}} \times \Gamma$ .

The structure of the parity-check matrix is kept in the lookup tables to provide the memory access indices. As in (8) to (10), the *a posteriori* LLR messages of the variable nodes in  $\mathbf{V}_{\text{layer}}$  as well as the check-to-variable LLRs in  $\mathbf{H}_{\text{layer}}$  will be accessed in the updating kernel. So two lookup tables are required. One lookup table  $LUT_c^{\text{layer}}$  is to record the indices of the check-to-variable messages associated with each check node and another table  $LUT_v^{\text{layer}}$  is to record the indices of the *a posteriori* LLRs of the variable nodes involved in the updating of each check node. Both lookup tables are two-dimensional and are similar to the ones in Type-A decoder.

### B. The GPU-based LDPCCC Decoder

The decoding algorithm and the pipelined LDPCCC decoder architecture have been introduced in Section II-C. The LDPCCCs studied in our work are derived from QC-LDPC codes as described in Section II-D. So our LDPCCC decoder is confined to the LDPCCCs with the parity-check matrix  $\mathbf{H}_{[0,\infty]}$  of this kind of structure.

#### Data Structure for the LDPCCC Decoder

The LDPC convolutional codes are decoded continuously. We will thus refer to a LDPCC code sequence  $\mathbf{v}_{[0,\infty]} = [\mathbf{v}_0, \mathbf{v}_1, \dots, \mathbf{v}_\infty]$  as a *code stream* and  $\mathbf{v}_i$ ,  $i = 0, 1, \dots, \infty$  as a *code frame* or *variable frame*. A code stream is constrained with the parity-check matrix  $\mathbf{H}_{[0,\infty]}$  by

$$\mathbf{v}_{[0,\infty]} \mathbf{H}_{[0,\infty]}^T = \mathbf{0}$$

The parity-check matrix of the LDPCCC is shown in Figure 7. It is seen that the check nodes are grouped into layers. Each variable-node frame is connected to  $m_s + 1$  (4 here) check layers in the parity-check matrix. Let  $c$  denote the size of  $\mathbf{v}_i$ ,  $i = 0, 1, \dots, \infty$  and  $c - b$  denote the size of each check layer. Thus the code rate is  $b/c$ .

We will use the same notations as in Section II-D. The LDPCCC is derived from a  $(J, L)$  QC-LDPC base code  $\mathbf{H}_{QC}$  which has  $J \times L$  sub-matrices and the size of each sub-matrix is  $p \times p$ .  $\mathbf{H}_{QC}$  is first

divided into  $\Lambda \times \Lambda$  sub-blocks<sup>3</sup> ( $\Lambda = 4$  in Figure 7) and each sub-block contains several sub-matrices. We have  $c = L/\Lambda \times p$  and  $c - b = J/\Lambda \times p$ . Referring to Section II-D, we denote the unwrapped parity-check matrix of the QC-LDPC code as

$$\mathbf{H}_{base} = \begin{bmatrix} \mathbf{H}_{QC}^L \\ \mathbf{H}_{QC}^U \end{bmatrix}.$$

The  $\mathbf{H}_{[0,\infty]}$  of the derived LDPCCC is a repetition of  $\mathbf{H}_{base}$ . Let  $E$  denote the number of edges in  $\mathbf{H}_{base}$  and  $E = J \times L \times p$ .

In designing the LDPCCC decoder, the first thing to consider is the amount of memory required to store the messages. Like the LDPC decoder, we store the messages according to the edges in the parity-check matrix. Let  $I$  denote the number of iterations in the LDPCCC decoding. Then  $I$  processors are required in the pipelined decoder. Although the parity-check matrix of the LDPCCC is semi-infinite, the decoder only needs to allocate memory for  $I$  processors. Hence the total size of the memory required for storing the messages passing between the variable nodes and check nodes is  $I \times E$  units. And the total size of the memory required for storing these channel messages is  $I \times c$ .

Next, we will describe the hierarchical data structure for the LDPCCC decoder memory space. To reuse the notation, we use  $\mathbf{H}$  to denote the memory space for the messages on the edges and  $\mathbf{V}$  to denote the memory space for the channel messages. The  $\mathbf{H}$  is a multi-dimensional array with two hierarchies. First, we divide the entire memory space into  $I$  groups corresponding to the  $I$  processors and we use the first hierarchy of  $\mathbf{H}$  as the data structure for each group. That is  $\mathbf{H}[i]$ ,  $i = 0, 1, \dots, I-1$  denote the data structure for the  $I$  processors, respectively. Second, recall that the parity-check matrix in Figure 7 is derived from  $\mathbf{H}_{base}$  which is divided into 16 non-zero sub-blocks and each sub-block has a size of  $(pJ/\Lambda) \times (pL/\Lambda)$ . Thus in each group,  $\mathbf{H}[i]$  is also divided into 16 sub-blocks, denoted by the second hierarchy of  $\mathbf{H}$ , namely,  $\mathbf{H}[i][j]$ , where  $j = 0, 1, \dots, 15$ . Every  $\mathbf{H}[i][j]$  stores the messages associated with one sub-block. On the other hand, the memory for the channel messages is simpler:  $\mathbf{V}[i]$ ,  $i = 0, 1, \dots, I \cdot (m_s + 1) - 1$  will be allocated. Finally, to optimize the thread execution and memory access,  $\Gamma$  LDPC convolutional code streams are decoded simultaneously, where  $\Gamma$  is a multiple of a warp. Thus every  $\Gamma$  data are combined into one package and take up one memory unit.

An LDPCCC decoder uses the BP algorithm to update the check nodes and variable nodes. The BP decoding procedures are based on the parity-check matrix  $\mathbf{H}_{[0,\infty]}$ . With the data structure to store the messages, the decoder also needs the structure information of  $\mathbf{H}_{[0,\infty]}$  for understanding the connections between the check nodes and the variable nodes. This information can be used to calculate the index of the data being accessed during the updating. Due to the periodic property of the constructed LDPCCC, the

<sup>3</sup>Note that a ‘‘sub-block’’ is different from a ‘‘sub-matrix’’.

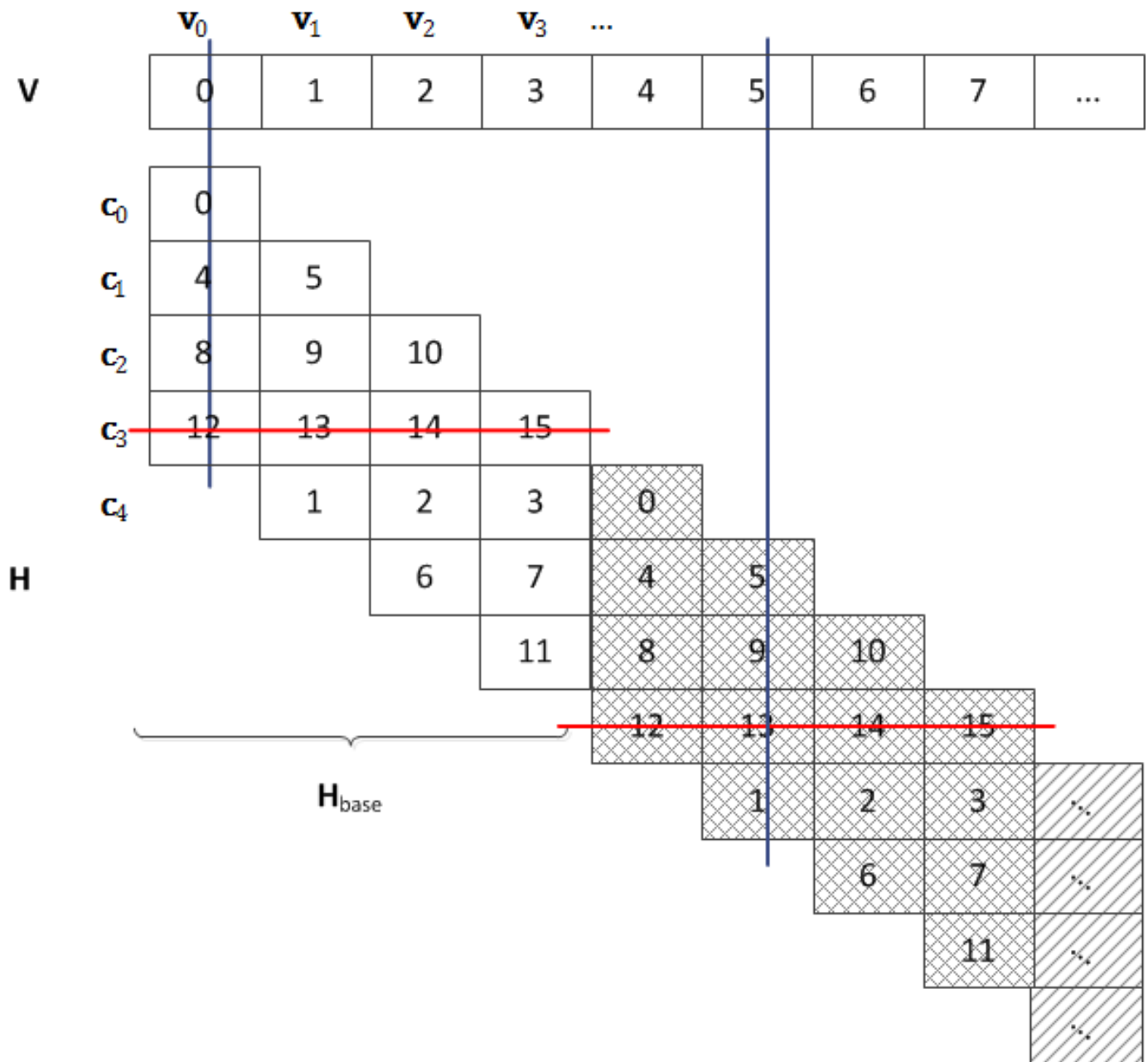


Fig. 7: The periodic structure of the parity-check matrix of the LDPCCCs.

structure of  $\mathbf{H}_{base}$  is shared by all the processors. We label the 16 sub-blocks in  $\mathbf{H}_{base}$  with the numbers  $0, 1, \dots, 15$ .

In addition, in the decoder, the  $I$  check-node layers or  $I$  variable-node frames being updated simultaneously in the  $I$  processors are separated by an interval of  $m_s + 1$ . Since  $\mathbf{H}_{[0,\infty]}$  also has a period of  $T = m_s + 1$ , at any time slot, the  $I$  processors require the same structure information in updating the check nodes or the variable nodes, as seen in Figure 7. The lookup tables used in check-node updating and variable-node updating are denoted as  $LUT_c$  and  $LUT_v$ , respectively. The two lookup tables will then

store the labels of the sub-blocks in  $\mathbf{H}_{base}$  that are involved in the updating process. Besides, another lookup table  $LUT_{sub}$  will be used to store the “shift numbers<sup>4</sup>” of the sub-matrices in each sub-block.

**Example 4.** The  $LUT_c$  and  $LUT_v$  for the LDPCCC in Figure 7 are

$$LUT_c = \begin{bmatrix} 1 & 2 & 3 & 0 \\ 6 & 7 & 4 & 5 \\ 11 & 8 & 9 & 10 \\ 12 & 13 & 14 & 15 \end{bmatrix} \quad (19)$$

and

$$LUT_v = \begin{bmatrix} 0 & 4 & 8 & 12 \\ 5 & 9 & 13 & 1 \\ 10 & 14 & 2 & 6 \\ 15 & 3 & 7 & 11 \end{bmatrix} \quad (20)$$

*Decoding Procedures with Parallel Thread Hierarchy:* Based on the discussion in Section II-E, the detailed decoding procedures are as follows.

- 1) At time slot 0, the first code frame  $\mathbf{v}_0$  enters Processor 1. This means the corresponding memory space  $\mathbf{V}[0]$  will be filled with the channel messages of  $\mathbf{v}_0$ . Then the channel messages will be propagated to the corresponding check nodes. Hence, referring to Fig. 7 and (20),  $\mathbf{H}[0][0]$ ,  $\mathbf{H}[0][4]$ ,  $\mathbf{H}[0][8]$  and  $\mathbf{H}[0][12]$  will be filled with the same channel messages  $\mathbf{V}[0]$ . Next, the first check layer of  $\mathbf{v}_0$ , i.e.,  $\mathbf{c}_0$ , will be updated based on the messages from  $\mathbf{v}_0$ , namely, the messages stored in  $\mathbf{H}[0][0]$  (they are the only messages available to  $\mathbf{c}_0$ ).
- 2) At time slot 1, the second code frame  $\mathbf{v}_1$  enters Processor 1. Hence the memory space  $\mathbf{V}[1]$ ,  $\mathbf{H}[0][5]$ ,  $\mathbf{H}[0][9]$ ,  $\mathbf{H}[0][13]$  and  $\mathbf{H}[0][1]$  will be filled with the messages of  $\mathbf{v}_1$ . Then, the check layer  $\mathbf{c}_1$  are updated in a similar way as the check layer  $\mathbf{c}_0$ . However, both the messages from  $\mathbf{v}_0$  and  $\mathbf{v}_1$ , i.e., messages stored in  $\mathbf{H}[0][4]$  and  $\mathbf{H}[0][5]$ , are used in the updating of  $\mathbf{c}_1$  based on the index information in  $LUT_c[1]$ . The procedure at time slot 1 is shown in Figure 8a.

The procedure goes on. When  $\mathbf{v}_3$  has been input and check layer  $\mathbf{c}_3$  has been updated, all the check-to-variable messages needed to update the variable layer  $\mathbf{v}_0$  are available. So  $\mathbf{v}_0$  will be updated with the channel messages in  $\mathbf{V}[0]$  and the check-to-variable messages in  $\mathbf{H}[0][0]$ ,  $\mathbf{H}[0][4]$ ,  $\mathbf{H}[0][8]$ , and  $\mathbf{H}[0][12]$ . Now,  $\mathbf{v}_0$  is now at the end of Processor 1 and is about to be shifted to Processor 2. Instead of copying the memory from one location to another, all we need to do is to specify that the memory  $\mathbf{v}_0$  “belongs” to Processor 2.

<sup>4</sup>For a QC-LDPC base matrix, the information is the “shift number” of each  $p \times p$  sub-matrix ( $-1$  represents the all-zero matrix,  $0$  represents the identity matrix,  $l$  represents cyclically right-shifting the identity matrix  $l$  times).

- 3) At the next time slot, i.e., time slot 4 (time slot  $m_s + 1$ ), the new code frame  $\mathbf{v}_4$  comes. The messages will be stored in  $\mathbf{v}[4]$  and  $\mathbf{H}[1][0]$ ,  $\mathbf{H}[1][4]$ ,  $\mathbf{H}[1][8]$  and  $\mathbf{H}[1][12]$ . Now there are two check layers to update,  $\mathbf{c}_0$  and  $\mathbf{c}_4$ . It is noted that  $\mathbf{c}_4$  are updated based on all the available messages in  $\mathbf{H}[0][1]$ ,  $\mathbf{H}[0][2]$ ,  $\mathbf{H}[0][3]$ , and  $\mathbf{H}[1][0]$  while  $\mathbf{c}_0$  are updated based on the updated messages only in  $\mathbf{H}[0][0]$ . This insufficient updating of check nodes only occurs to the first  $m_s$  code frames. After the updating of the check nodes, the code frame  $\mathbf{v}_1$  is at the end of Processor 1 and will be updated. There is no code frame arriving at the end of Processor 2 yet.
- 4) At time slot  $I \cdot (m_s + 1) - 1$ , the entire memory space of  $\mathbf{V}$  and  $\mathbf{H}$  are filled with messages.  $\mathbf{v}_0$  and its associated messages are at the end of Processor  $I$  (as being labeled) while  $\mathbf{v}_{i \cdot (m_s + 1) - 1}$  is the latest code frame input into Processor 1. Next, the check nodes in the  $I$  check layers of the  $I$  processors will be updated in parallel. After the updating of the check nodes, all the variable nodes which are leaving Processor  $i$  ( $i = 1, 2, \dots, I$ ) are updated. Specifically, the variable nodes  $\mathbf{v}_{i \cdot (m_s + 1) - 1}$ ,  $i = 1, 2, \dots, I$  are to be updated. Furthermore,  $\mathbf{v}_0$  is about to leave the decoder. Hard decision will be made based on the *a posteriori* LLR of  $\mathbf{v}_0$ . Then the memory space of  $\mathbf{v}_0$ ,  $\mathbf{V}[0]$ ,  $\mathbf{H}[0][0]$ ,  $\mathbf{H}[0][4]$ ,  $\mathbf{H}[0][8]$  and  $\mathbf{H}[0][12]$  are cleared for reuse. At the next time slot  $I \cdot (m_s + 1)$ , the new code frame  $\mathbf{v}_{I \cdot (m_s + 1)}$  comes in the decoder and these memory space will be filled with the messages of  $\mathbf{v}_{I \cdot (m_s + 1)}$ .

**Remark.** *In our GPU-based decoder, all the check nodes (variable nodes) needed to be updated in the  $I$  processors are processed in parallel by multiple threads.*

- 5) Note that the LDPC matrix has a period of  $T = m_s + 1$  (4 here). Hence, at time slot  $t \geq I \cdot (m_s + 1)$ ,  $\mathbf{v}_t$  enters the decoder and reuses the memory space of  $\mathbf{v}_\tau$  where  $\tau = t \bmod (I \cdot (m_s + 1))$ . Furthermore, we let  $\kappa = t \bmod (m_s + 1)$ . Then the check layer  $\mathbf{c}_{\kappa + (i-1) \cdot (m_s + 1)}$  in Processor  $i$  ( $i = 1, 2, \dots, I$ ) will be updated followed by the updating of the code frame  $\mathbf{v}_{\kappa + i \cdot (m_s + 1) - m_s}$ . Moreover, the “oldest” code frame residing in the decoder —  $\mathbf{v}_{t - I \cdot (m_s + 1)}$  — is about to leave the decoder and hard decisions will be made on it.

So the entire LDPC decoder possesses a circulant structure, as shown in Figure 9. The memory is not shifted except for the one associated with the code frame which is leaving the decoder. Instead, the processor are “moving” by changing the processor label of each code frame. Correspondingly, the “entrance” and “exit” are moving along the data structure. This circulant structure reduces the time for memory manipulation and simplifies the decoder.

As described in the data structure, the memory associated with each entry in the  $\mathbf{H}$  matrix is a message package containing  $\Gamma$  messages from  $\Gamma$  code streams. So there is a straightforward mapping between the thread hierarchy and the data structure. In the check-node-updating kernel (or

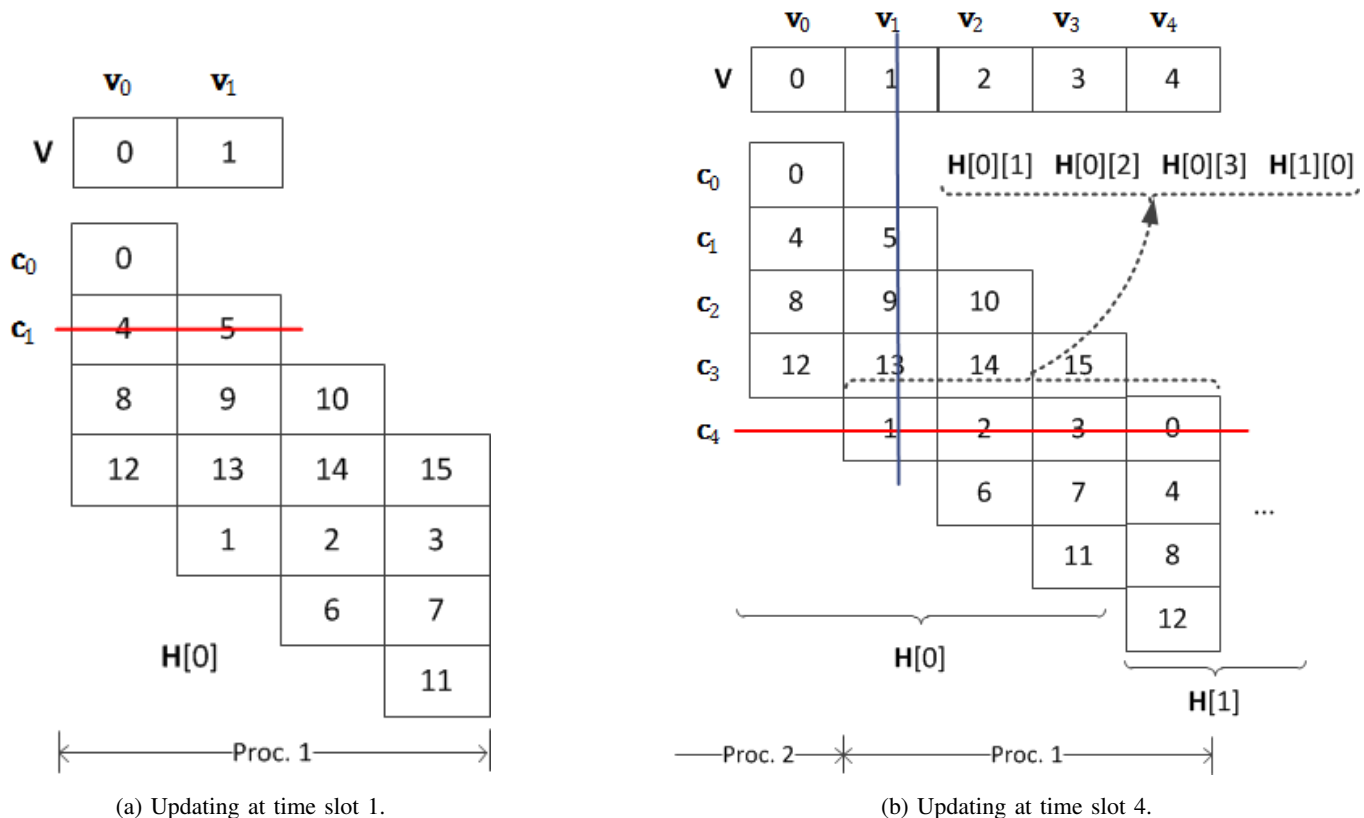


Fig. 8: Illustration of the procedures of a LPDCCC decoder. The horizontal line denotes the updating of the row. The vertical line denotes the updating of a column.

variable-updating-kernel), a two dimensional thread hierarchy of size  $I \cdot (c - b) \times \Gamma$  (or  $I \cdot c \times \Gamma$ ) is launched, where  $(c - b)$  (or  $c$ ) is mapped to the total number of check nodes (or variable nodes) being updated in  $I$  processors. The size of one of the dimensions (i.e.,  $\Gamma$ ) is mapped to the number of code streams. Like in LDPC decoder,  $\Gamma$  will be configured as the *threadIdx.x* dimension and  $(c - b)$  (or  $c$ ) will be the *threadIdx.y* dimension in the CUDA thread hierarchy. The  $\Gamma$  threads in the *threadIdx.x* dimension is contiguous and will access the  $\Gamma$  data in each message package for coalesced access.

## V. RESULTS AND DISCUSSION

### A. The Experimental Environment

We compare the results of the proposed GPU-based LDPC decoder with that of a CPU-based decoder. The CPU-based decoder is developed using C programming and the commonly used linked-list approach is employed to store and link the messages [2]. Details of the CPU and GPU used in our simulations are presented in Table I. Note that although there are 8 cores in the CPU, simple C programming (without

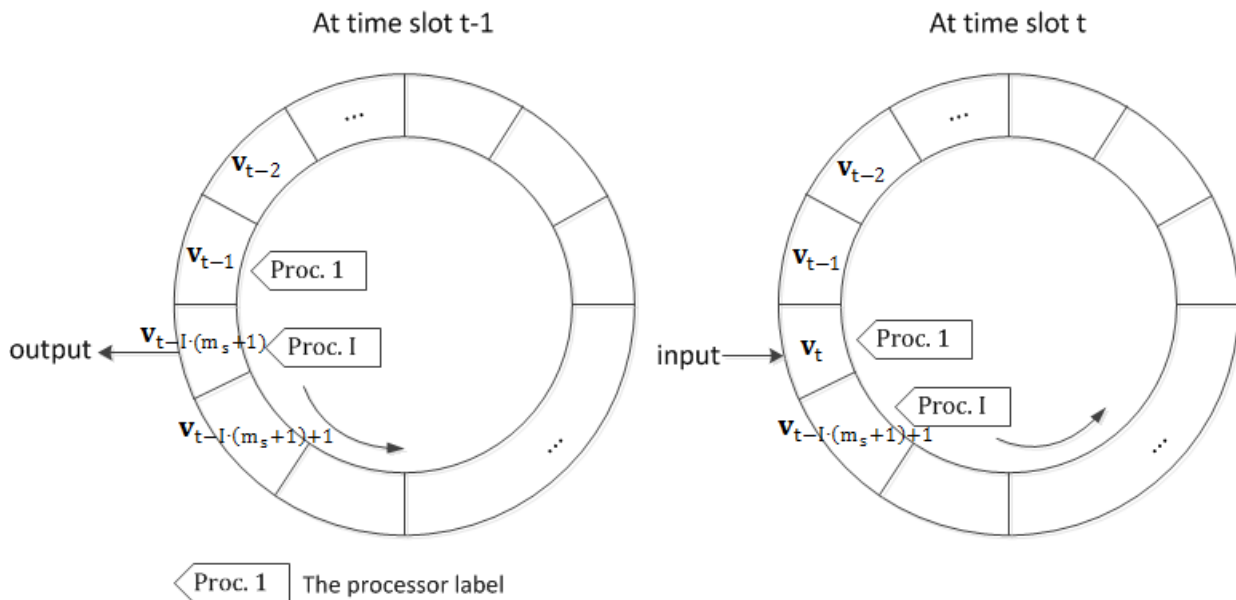


Fig. 9: Illustration of the circulant structure of LPDCCC decoder.

	CPU	GPU
Platform	Intel Xeon	Nvidia GTX460
Number of cores	8 (only one core used)	$7 \times 48 = 336$
Clock rate	2.26 GHz	0.81 GHz
Memory	8 GB DDR3 RAM	768 MB global memory and 48 KB shared memory
Maximum Thread-block size	—	1024 threads
Programming Language	C	CUDA C

TABLE I: Simulation environments.

parallel computing) allows us to use only one of the cores. Table II shows the characteristics of the QC-LDPC codes under test. For Code A to code D,  $J = 4$  and  $L = 24$  thus giving the same code rate of  $(24 - 4)/24 = 5/6$ .

For the LPDCCC decoder, in Table III, the characteristics of the LDPC convolutional codes derived from the QC-LDPC codes are listed. In order to avoid confusion, we denote the QC-LDPC code as code A, code B, etc., while the derived LPDCCCs as code A', code B', etc., respectively. The  $(m_s, J, K)$ -LPDCCCs A' to D' derived from the  $(4, 24)$ -QC-LDPC codes A to D are  $(3, 4, 24)$  regular LDPC convolutional codes with the same code rate of  $(24 - 4)/24 = 5/6$ .

Code	$J \times L$	Sub-matrix size ( $p \times p$ )	Parity-Check Matrix Size ( $M \times N$ )	Number of Edges ( $M \times L$ or $N \times J$ )
A	$4 \times 24$	$422 \times 422$	$1688 \times 10128$	40512
B	$4 \times 24$	$632 \times 632$	$2528 \times 15168$	60672
C	$4 \times 24$	$765 \times 765$	$3060 \times 18360$	73440
D	$4 \times 24$	$1024 \times 1024$	$4096 \times 24576$	98304

TABLE II: Parity-check matrices of the QC-LDPC codes under test.

Code	$J \times L$	$p$	$c \times (c - b)$	Number of Edges
A'	$4 \times 24$	422	$2532 \times 422$	40512
B'	$4 \times 24$	632	$3792 \times 632$	60672
C'	$4 \times 24$	768	$4608 \times 768$	73728
D'	$4 \times 24$	1024	$6144 \times 1024$	98304

TABLE III: Parity-check matrices of the QC-LDPC codes used to derive the LDPCCCs.

### B. The BER Simulation Results

For the LDPC decoders, the bit error rate (BER) curves of Code A and Code D are shown in Fig. 10. The BER results of the GPU-based Type-A decoder using standard BP algorithm as well as the Type-B decoder using layered algorithm are plotted and compared with the result of the CPU-based decoder using standard BP algorithm. The  $E_b/N_0$  ranges from 2.7 dB to 3.3 dB. It can be observed that the BER performance of the CPU- and GPU-based decoders with the BP algorithm is very close under the same number of iterations 30. Meanwhile, the layered decoder reaches the same BER performance with half the number of iterations, i.e., 15. The observation implies that the layered decoding algorithm converges twice the speed of the standard one.

**Remark.** Note that although QC-LDPC codes are adopted in the simulation, the new GPU-based LDPC decoder is able to decode other LDPC codes like randomly-constructed regular or irregular codes.

For the LDPCCC decoder, we compare the bit error rate (BER) results of the GPU-based decoder with the results of the CPU-based decoder in Fig. 11. Code A' and code D' are decoded with 15 iterations, i.e., there are  $I = 15$  processors. It is seen that the results of the GPU-based decoder tally with the ones of the CPU-based decoder. Besides, the BER performance of the LDPCCCs are much better than the counterpart LDPC block codes as shown in Fig. 12. Code A and Code D LDPC block codes are compared with the

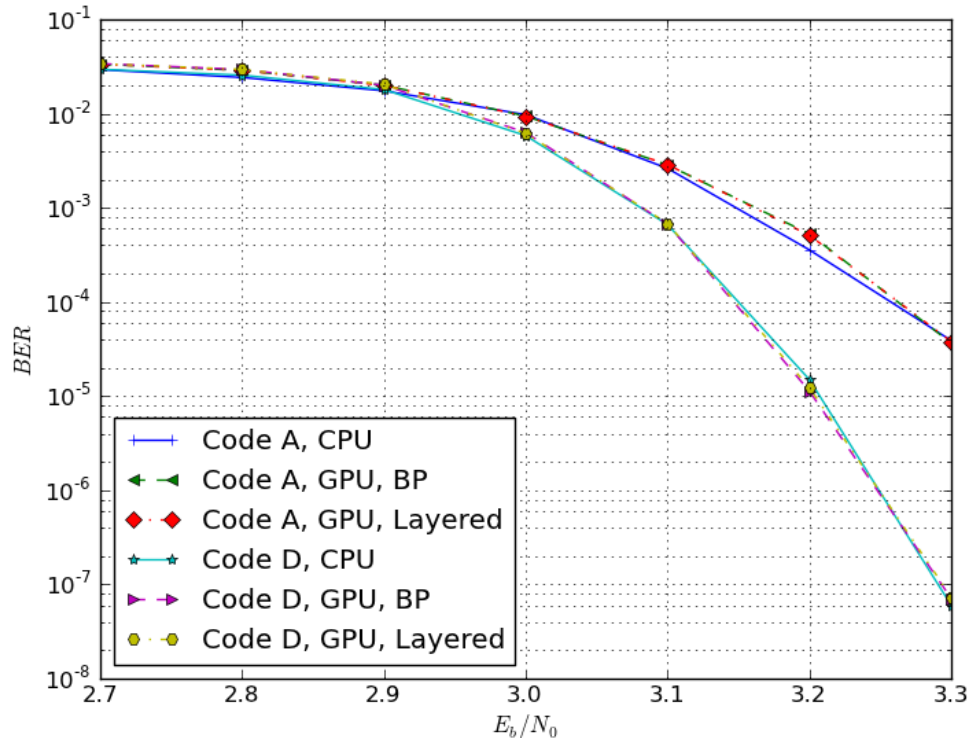


Fig. 10: BER performance of the GPU-based Type-A decoder (using the standard BP algorithm), Type-B decoder (using the layered decoding algorithm) and CPU-based BP decoder. 30 iterations are used for the standard BP decoder while 15 iterations are used for the layered one.

corresponding Code A' and Code D' LDPCs. The LDPC block codes are decoded with 15 standard BP iterations while there are  $I = 15$  processors for the LDPC decoder. It can be seen that at the BER level of  $10^{-5}$ , the  $E_b/N_0$ 's of Code A' is lower than the one of Code A by about 0.2 dB. For Code D' and Code D, there is also a difference of 0.2 dB at a BER of  $10^{-7}$ .

### C. The Decoding Time Comparison

In the following, we fix the number of decoding iterations and the simulation terminates after 100 (codeword) block errors are received. Since the block/bit error rate (BLER/BER) decreases with the bit-energy-to-noise-power-spectral-density ratio ( $E_b/N_0$ ), the total simulation time taken to obtain the same number of block errors increases with  $E_b/N_0$ . Nonetheless, the average time taken to decode one codeword should remain the same.

Table IV shows the number of transmitted codewords and the simulation times for different codes when the CPU-based and the GPU-based decoders are used. Note that the number of decoded codewords increases from Code A to Code D due to decreasing of the BLER.

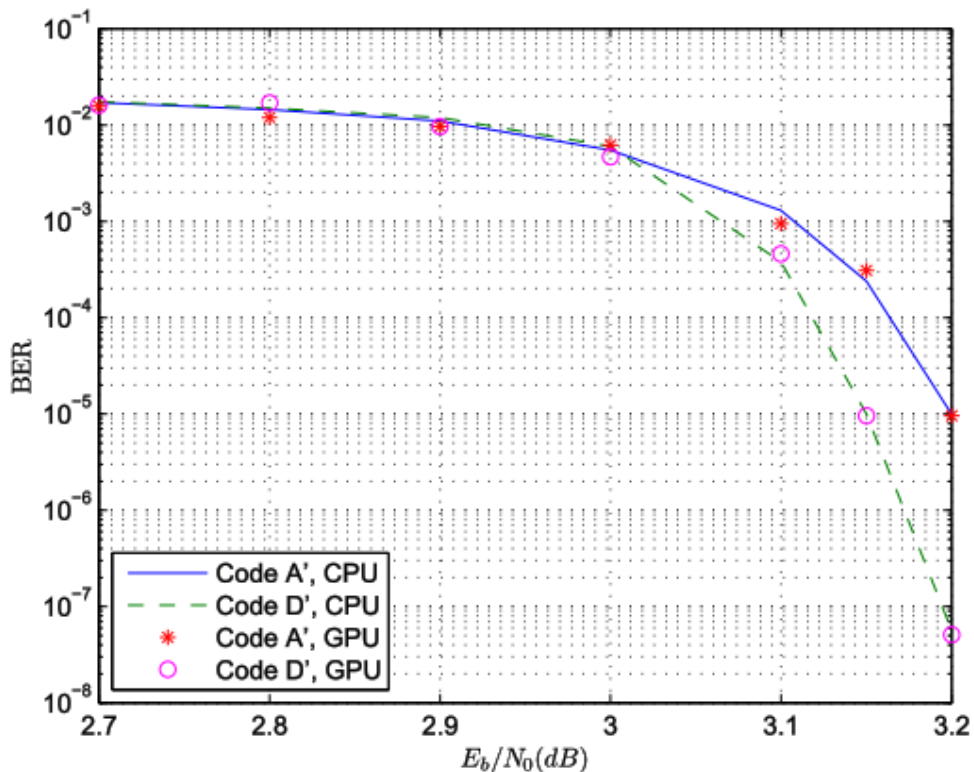


Fig. 11: The BER of the LDPCCC decoder based on the GPU and CPU.  $I = 15$  processors.

We consider the average time for decoding one codeword for the CPU-based decoder, i.e.,  $t_{\text{CPU}}$ . We observe that  $t_{\text{CPU}}$  increases from Code A to Code D due to the different number of edges. Further, we consider the average time for decoding one codeword for the GPU-based decoders, i.e.,  $t_{\text{GPU}}$ . Similar to the CPU-based decoder,  $t_{\text{GPU}}$  increases from Code A to Code D. The decoding times per codeword are listed in Table IV. The two standard BP decoders are tested with 30 iterations at the  $E_b/N_0$  of 3.2 dB while the layered one is executed with 15 iterations at the same  $E_b/N_0$ . Although the iteration number of the decoder with layered algorithm is half of the standard one, the comparison is reasonable since they attain the same BER level. Finally, we compare the simulation times of the CPU-based decoder and the GPU-based decoders by taking the ratio  $t_{\text{CPU}}/t_{\text{GPU}}$ . The results in Table IV indicate that the GPU-based Type-A decoder with the standard BP decoding algorithm accomplishes speedup improvements from 148 times to 162 times compared with the CPU-based decoder with BP decoding algorithm. Besides, the Type-B decoder with the layered decoding algorithm can further speed up the simulation.

Moreover, the decoding time of the LDPCCC decoders based on CPU and GPU are compared in Table V. All the LDPC convolutional codes A' to D' are decoded at a  $E_b/N_0$  of 3.1 dB with  $I = 20$ . We observe that the GPU-based LDPCCC decoder can achieve 170 ~ 200 times speedup improvement.

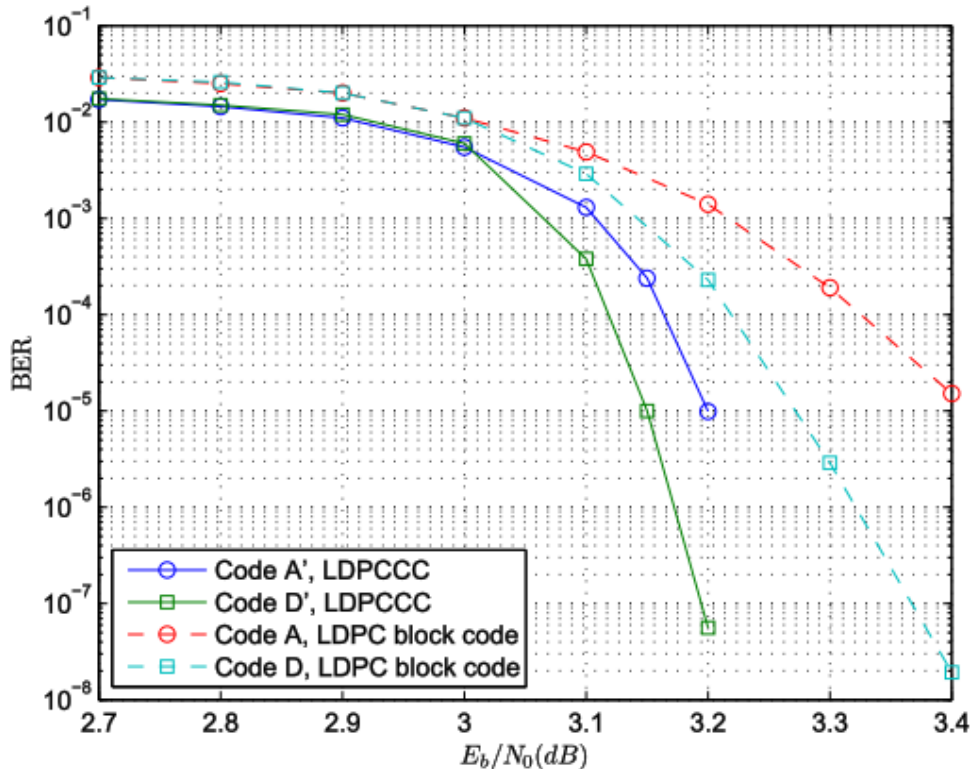


Fig. 12: The BER performance of the LDPCCCs and the base QC-LDPC codes.  $I = 15$ .

Code	$C_{CPU}$	$T_{CPU}$ (s)	$t_{CPU}$ (ms)	$C_A$	$T_A$ (s)	$t_A$ (ms)	Speedup $(\frac{t_{CPU}}{t_A})$	$C_B$	$T_B$ (s)	$t_B$ (ms)	Speedup $(\frac{t_{CPU}}{t_B})$
A	4058	1270	313	2832	6	2.12	148	3072	4	1.3	241
B	11664	5350	458	12768	37	2.9	158	12800	23	1.8	254
C	20046	10950	546	21664	74	3.4	161	22400	46	2.05	266
D	70843	51580	728	82624	371	4.5	162	82640	228	2.76	264

TABLE IV: Decoding time per codeword for the GPU-based LDPC decoders at  $E_b/N_0=3.2$  dB. 30 iterations are used for Type-A decoder while 15 iterations are used for the Type-B decoder.  $C$  represents the total number of decoded codewords;  $T$  denotes the total simulation time and  $t$  is the average simulation time per codeword. The subscript "A" stands for Type-A GPU decoder and "B" for Type-B GPU decoder.

## VI. CONCLUSION

In this paper, efficient decoders for LDPC codes and LDPC convolutional codes based on the GPU parallel architecture are implemented. By using efficient data structure and thread layout, the thread divergence is avoided and the memory can be accessed in a coalesced way. All decoders are flexible and

Code	$C_{GPU}$	$T_{GPU}$ (s)	$t_{GPU}$ (ms)	$C_{CPU}$	$T_{CPU}$ (s)	$t_{CPU}$ (ms)	Speedup $(\frac{t_{CPU}}{t_{GPU}})$
A'	3136	0.73	0.23	2846	112	39	169
B'	6272	1.95	0.31	5716	345	60	194
C'	14400	5.4	0.38	13303	976	73	195
D'	43680	21.0	0.48	37451	3590	96	200

TABLE V: Decoding time per code frame.  $C$  represents the total number of decoded frames;  $T$  denotes the total simulation time;  $t$  is the average simulation time per frame.  $E_b/N_0 = 3.1$  dB and  $I = 20$  processors.

scalable. First, they can decode different codes by changing the parameters. Hence, the programs need very little modification. Second, they can run on the latest or even future generations of GPUs which possess more hardware resources. These are actually advantages of GPU parallel architecture compared to other parallel solutions including FPGA or VLSI. Compared with the traditional CPU-based decoders, results show that the proposed GPU-based decoders can achieve  $100\times \sim 200\times$  speed-up. The actual time depends on the particular decoder and codes. Thus a one-week CPU-based simulation can be reduced to less than one hour when a GPU-based decoder is used.

## REFERENCES

- [1] R. G. Gallager, *Low-Density Parity-Check Codes*. The MIT Press, Sep. 1963.
- [2] D. MacKay, "Good error-correcting codes based on very sparse matrices," *Information Theory, IEEE Transactions on*, vol. 45, no. 2, pp. 399–431, 1999.
- [3] I. Djordjevic, M. Cvijetic, L. Xu, and T. Wang, "Using LDPC-Coded modulation and coherent detection for ultra highspeed optical transmission," *Lightwave Technology, Journal of*, vol. 25, no. 11, pp. 3619–3625, 2007.
- [4] Y. Miyata, K. Sugihara, W. Matsumoto, K. Onohara, T. Sugihara, K. Kubo, H. Yoshida, and T. Mizuochi, "A triple-concatenated FEC using soft-decision decoding for 100 Gb/s optical transmission," in *Optical Fiber Communication (OFC), collocated National Fiber Optic Engineers Conference, 2010 Conference on (OFC/NFOEC)*, 2010, pp. 1–3.
- [5] Y. Chen and D. Hocevar, "A FPGA and ASIC implementation of rate 1/2, 8088-b irregular low density parity check decoder," in *Global Telecommunications Conference, 2003. GLOBECOM '03. IEEE*, vol. 1, 2003, pp. 113–117 Vol.1.
- [6] I. B. Djordjevic, M. Arabaci, and L. L. Minkov, "Next generation FEC for High-Capacity communication in optical transport networks," *Journal of Lightwave Technology*, vol. 27, no. 16, pp. 3518–3530, 2009.
- [7] B. Levine, R. R. Taylor, and H. Schmit, "Implementation of near Shannon limit error-correcting codes using reconfigurable hardware," 2000.
- [8] G. Falcao, V. Silva, and L. Sousa, "How GPUs can outperform ASICs for fast LDPC decoding," in *Proceedings of the 23rd international conference on Supercomputing*. Yorktown Heights, NY, USA: ACM, 2009, pp. 390–399.
- [9] H. Ji, J. Cho, and W. Sung, "Massively parallel implementation of cyclic LDPC codes on a general purpose graphics processing unit," in *Signal Processing Systems, 2009. SiPS 2009. IEEE Workshop on*. IEEE, 2009, pp. 285–290.
- [10] —, "Memory access optimized implementation of cyclic and quasi-cyclic LDPC codes on a GPGPU," *Journal of Signal Processing Systems*, pp. 1–11, 2010.

- [11] G. Falcao, L. Sousa, and V. Silva, "Massive parallel LDPC decoding on GPU," in *Proceedings of the 13th ACM SIGPLAN Symposium on Principles and practice of parallel programming*. Salt Lake City, UT, USA: ACM, 2008, pp. 83–90.
- [12] A. J. Felstrom and K. Zigangirov, "Time-varying periodic convolutional codes with low-density parity-check matrix," *Information Theory, IEEE Transactions on*, vol. 45, no. 6, pp. 2181–2191, 1999.
- [13] M. Tavares, E. Matus, S. Kunze, and G. Fettweis, "A dual-core programmable decoder for LDPC convolutional codes," in *Circuits and Systems, 2008. ISCAS 2008. IEEE International Symposium on*, May 2008, pp. 532–535.
- [14] E. Matus, M. Tavares, M. Bimberg, and G. Fettweis, "Towards a GBit/s programmable decoder for LDPC convolutional codes," in *Circuits and Systems, 2007. ISCAS 2007. IEEE International Symposium on*, May 2007, pp. 1657–1660.
- [15] R. Tanner, "A recursive approach to low complexity codes," *Information Theory, IEEE Transactions on*, vol. 27, no. 5, pp. 533–547, 1981.
- [16] M. Fossorier, "Quasicyclic low-density parity-check codes from circulant permutation matrices," *Information Theory, IEEE Transactions on*, vol. 50, no. 8, pp. 1788–1793, 2004.
- [17] W. Tam, F. Lau, and C. Tse, "A class of QC-LDPC codes with low encoding complexity and good error performance," *Communications Letters, IEEE*, vol. 14, no. 2, pp. 169–171, 2010.
- [18] T. Richardson, M. Shokrollahi, and R. Urbanke, "Design of capacity-approaching irregular low-density parity-check codes," *Information Theory, IEEE Transactions on*, vol. 47, no. 2, pp. 619–637, 2001.
- [19] T. Richardson and R. Urbanke, "Efficient encoding of low-density parity-check codes," *Information Theory, IEEE Transactions on*, vol. 47, no. 2, pp. 638–656, 2001.
- [20] X. Hu, E. Eleftheriou, D. Arnold, and A. Dholakia, "Efficient implementations of the sum-product algorithm for decoding LDPC codes," in *Global Telecommunications Conference, 2001. GLOBECOM '01. IEEE*, vol. 2, 2001, pp. 1036–1036E vol.2.
- [21] J. Chen, A. Dholakia, E. Eleftheriou, M. Fossorier, and X. Hu, "Reduced-Complexity decoding of LDPC codes," *Communications, IEEE Transactions on*, vol. 53, no. 8, pp. 1288–1299, 2005.
- [22] D. Hocevar, "A reduced complexity decoder architecture via layered decoding of LDPC codes," in *Signal Processing Systems, 2004. SIPS 2004. IEEE Workshop on*, 2004, pp. 107–112.
- [23] R. Tanner, D. Sridhara, A. Sridharan, T. Fuja, and D. Costello, "LDPC block and convolutional codes based on circulant matrices," *Information Theory, IEEE Transactions on*, vol. 50, no. 12, pp. 2966–2984, 2004.
- [24] A. E. Pusane, R. Smarandache, P. O. Vontobel, and D. J. Costello, "On deriving good LDPC convolutional codes from QC-LDPC block codes," in *Proc. IEEE Int. Symp. Information Theory ISIT 2007*, 2007, pp. 1221–1225.
- [25] M. Lentmaier, D. G. M. Mitchell, G. P. Fettweis, and D. J. Costello, "Asymptotically regular LDPC codes with linear distance growth and thresholds close to capacity," in *Proc. Information Theory and Applications Workshop (ITA)*, 2010, pp. 1–8.
- [26] C. Nvidia, "Compute Unified Device Architecture Programming Guide Version 4.0," NVIDIA Corporation, Tech. Rep., 2011.
- [27] W. Nvidia, N. Generation, and C. Compute, "Whitepaper nvidia's next generation cuda compute architecture," *ReVision*, pp. 1–22, 2009.
- [28] F. Kschischang, B. Frey, and H. Loeliger, "Factor graphs and the sum-product algorithm," *Information Theory, IEEE Transactions on*, vol. 47, no. 2, pp. 498–519, 2001.